applied sciences

MDPI

Article

Model Predictive Control for Six-Phase Induction Machines with Insight into Past Current Errors

Juan Carrillo-Ríos [1,*], Ignacio González-Prieto [1], Ángel González-Prieto [2], Mario J. Durán [1] and Juan José Aciego [1]

[1] Departamento de Ingenieria Electrica, Escuela de Ingenierias Industriales, Universidad de Malaga, 29010 Malaga, Spain; igp@uma.es (I.G.-P.); mjduran@uma.es (M.J.D.); juanjoseaciego@uma.es (J.J.A.)
[2] Departamento de Ingenieria Electrica, Escuela Tecnica Superior de Ingenierias Industriales, Universidad Politecnica de Madrid, 28040 Madrid, Spain; angel.gprieto@upm.es
* Correspondence: juan.carrillo.rios@uma.es

Abstract: Multi-phase electric drives can act as a competitive solution for high-power applications. To take advantage of the multi-phase benefits, the design of high-performance control techniques is a crucial task. In this regard, the inherent features of model predictive control (MPC) have aroused the interest of the scientific community in the last decade. This control solution, based on the usage of a cost function, provides notable flexibility to the control designer to select diverse regulation goals. Although the use of some weighting factors is a common trend to prioritize control purposes, the internal behavior of each term of the cost function is commonly ignored since the cost function is only focused on minimizing the total error. With this issue in mind, this work firstly performs a detailed analysis about the behavior of each cost function term in a standard MPC. The mentioned study permits identifying a certain pattern of the internal mechanics of the cost function that can disturb the current quality. To solve this limitation, the cost function of the MPC scheme is redefined. The proposed strategy permits improving current quality without increasing the number of switching states applied per control period, as it is validated with experimental results in six-phase electric drives.

Keywords: accumulation of current errors; cost function; finite control set model predictive control; multi-phase electric drives

check for updates

Citation: Carrillo-Ríos, J.; González-Prieto, I.; González-Prieto, A.; Durán M.J.; Aciego, J.J. Model Predictive Control for Six-Phase Induction Machines with Insight into Past Current Errors. *Appl. Sci.* **2024**, *14*, 11684. https://doi.org/10.3390/app142411684

Academic Editor: Muhammad Aziz

Received: 8 November 2024
Revised: 8 December 2024
Accepted: 12 December 2024
Published: 14 December 2024

Copyright: © 2024 by the authors. Licensee MDPI, Basel, Switzerland. This article is an open access article distributed under the terms and conditions of the Creative Commons Attribution (CC BY) license (https://creativecommons.org/licenses/by/4.0/).

1. Introduction

Multi-phase electric machines present an interesting solution for industrial applications when high power and reliability are required [1–3]. Even though the early development of these systems was thwarted by their inherent complexity in terms of control, the progress of digital signal processors has alleviated this problem [4]. Better power distribution, fault-tolerant capabilities, and lower torque ripple are some of the advantages that these machines present over their three-phase counterparts [5]. An example of this fact is that the impact of multi-phase systems on the field of electric vehicles is not limited to academic studies [6–8]. Companies such as BMW, Mercedes, and Audi have incorporated propulsion systems with multi-phase solutions into some of their high-end products [9–11].

Regarding the regulation of multi-phase electric drives, different control techniques have been extended from three-phase systems. Such is the case with indirect rotor field-oriented control [12,13], direct torque control [14,15], and finite control set model predictive control (FCS-MPC) [16–18] for both induction and permanent magnet synchronous machines [19,20]. This last regulation scheme has gained traction in the last decade thanks to its high usage of the dc-link voltage, fast dynamic response, and inherent flexibility in adding specific control goals in a simple manner [4]. Despite these benefits, FCS-MPC presented a serious limitation in its early development, showing poor current quality for low values of stator impedance when only one switching state is applied per control action [4].

One possible approach to improve the current quality is the use of multi-vector solutions, which have been explored for systems with three phases [21], but also five [21–23], six [4,24,25], and nine phases [26], among others. By adequately composing new control actions from applying multiple switching states in one sampling period, currents in the secondary subspace can be significantly reduced, thus enhancing the machine performance. Nevertheless, this solution is not without its faults. First of all, applying a higher number of switching states comes at a dual cost: a higher switching frequency and a lower usage of the dc-link voltage [4,27]. Furthermore, the reduction in currents in the secondary plane comes in part from the higher switching rate. Smaller sampling times inherently lead to an increase in switching frequency, and consequently, the difference in performance between a multi-vector solution and a standard FCS-MPC could reduce. This fact can be especially notable if the control actions of the standard FCS-MPC are pre-selected to ensure a low production of secondary currents [4].

Due to both the advantages and disadvantages of using multi-vector solutions, these schemes coexist with FCS-MPCs that only use one switching state. Some of the single-switching state regulation schemes focus on alternative control goals, such as enhancing current tracking [28], decreasing the VSC switching frequency [27,29] or mitigating common-mode voltages [30]. These objectives are pursued through the modification of the cost function that governs the selection of control actions, which is the source of the FCS-MPC's flexibility.

Nevertheless, regardless of the number of switching states applied per control period, when FCS-MPC is trying to reduce current errors, the cost function is only focused on minimizing the total error. This leaves the door open for the individual growth of the different current errors as long as the sum is somewhat compensated in the present control cycle. This behavior could present a blind spot in the control's ability to keep all errors low. Particularly, the sensitivity of the secondary subspace could lead to the accumulation of current errors through many cycles, worsening the system's performance. The present work contains two contributions (C1 and C2) that, to the best of the authors' knowledge, are novel.

On the one hand, C1 aims to fill in the research gap present in the field of FCS-MPC: how the individual errors that make up the cost function evolve through time during standard functioning conditions. A study of these current errors is presented based on experimental tests, providing archival value and demonstrating a flaw in this type of control scheme that has not been explored before, but can be solved. On the other hand, C2 is a novel and cost-effective solution to said flaw: a redefined FCS-MPC which targets a reduction in the accumulated error of the available components. By doing so, current harmonic injection is notably reduced without increasing switching frequency. Furthermore, the limitations that the proposed control scheme presents have been explored, paying special attention to the increase in computational time and complexity.

The manuscript is structured as follows. Section 2 reviews the generalities of the multi-phase topology used in this work, whereas Section 3 details the functioning of standard FCS-MPC and how individual current errors evolve during its performance. Section 4 proposes an alternative MPC algorithm focused on the reduction in accumulated error (RAE-MPC), and Section 5 compares its results with standard FCS-MPC, exploring both advantages and disadvantages between the control schemes. The conclusions obtained in the presented work are detailed in Section 6.

2. The Six-Phase Induction Motor Drive

The employed electric drive is composed of a double three-phase two-level voltage source converter (VSC) connected to an asymmetrical six-phase induction machine (IM) [31]. The IM stator windings have been configured with isolated neutral points, simplifying the complexity of the control scheme [32]. A general diagram of the system's topology is shown in Figure 1. Every VSC leg is formed by two complementary switches that determine the switching state of each of the six phases, adding up to $2^6 = 64$ possible states (S_{ph_j}), where the subscript "ph" and "j" refer to the phase (a, b, and c) and the VSC it belongs to

(1 or 2), respectively. The complementary switches behave in a binary manner, with $S_{ph_j} = 1$ resulting in the upper switch being ON and the lower switch being OFF. Consequently, $S_{ph_j} = 0$ entails the opposite behavior for upper and lower switches. The expression (1) defines the stator phase voltages (v_{ph_j}) obtained in the considered electric drive:

$$\begin{bmatrix} v_{a1} \\ v_{b1} \\ v_{c1} \\ v_{a2} \\ v_{b2} \\ v_{c2} \end{bmatrix} = \frac{V_{dc}}{3} \begin{bmatrix} 2 & -1 & -1 & 0 & 0 & 0 \\ -1 & 2 & -1 & 0 & 0 & 0 \\ -1 & -1 & 2 & 0 & 0 & 0 \\ 0 & 0 & 0 & 2 & -1 & -1 \\ 0 & 0 & 0 & -1 & 2 & -1 \\ 0 & 0 & 0 & -1 & -1 & 2 \end{bmatrix} \begin{bmatrix} S_{a_1} \\ S_{b_1} \\ S_{c_1} \\ S_{a_2} \\ S_{b_2} \\ S_{c_2} \end{bmatrix}, \tag{1}$$

where V_{dc} is the voltage provided by the dc-link.

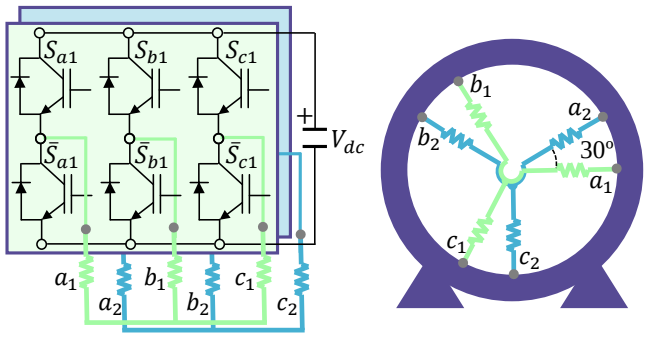


Figure 1. Topology of the asymmetrical six-phase IM with a double three-phase two-level VSC.

Even though expressing IM behavior in phase variables is a common practice, the use of different reference frames can facilitate control design. An example is the use of vector space decomposition (VSD) which, in the case of the six-phase machine, maps phase stator values onto three orthonormal subspaces with distinct physical meaning [33]. This useful transformation is achieved through the use of the Clarke matrix (2). The primary plane is the α-β subspace, which is related to flux and torque production. The secondary plane is the x-y subspace, and it maps the harmonic components that produce copper losses in distributed winding machines as long as the spatial harmonics are negligible. The last product of the use of the Clarke transform are the zero-sequence currents which, due to the fact that the neutral points of the studied system are isolated, can be considered zero and thus ignored.

$$[C] = \frac{1}{3} \begin{bmatrix} 1 & -\frac{1}{2} & -\frac{1}{2} & \frac{\sqrt{3}}{2} & -\frac{\sqrt{3}}{2} & 0 \\ 0 & \frac{\sqrt{3}}{2} & -\frac{\sqrt{3}}{2} & \frac{1}{2} & \frac{1}{2} & -1 \\ 1 & -\frac{1}{2} & -\frac{1}{2} & -\frac{\sqrt{3}}{2} & \frac{\sqrt{3}}{2} & 0 \\ 0 & -\frac{\sqrt{3}}{2} & \frac{\sqrt{3}}{2} & \frac{1}{2} & \frac{1}{2} & -1 \\ 1 & 1 & 1 & 0 & 0 & 0 \\ 0 & 0 & 0 & 1 & 1 & 1 \end{bmatrix}, \tag{2}$$

$$[x_\alpha \ x_\beta \ x_x \ x_y \ x_{z1} \ x_{z2}]^T = [C][x_{a1} \ x_{b1} \ x_{c1} \ x_{a2} \ x_{b2} \ x_{c2}]^T, \tag{3}$$

where x can represent the current, the voltage or the flux of the electric machine.

Using standard assumptions [2], the employed six-phase IM can be modeled as follows:

$$
\begin{aligned}
v_\alpha &= (R_s + L_s\frac{d}{dt})i_{\alpha s} + M\frac{di_{\alpha r}}{dt},\\
v_\beta &= (R_s + L_s\frac{d}{dt})i_{\beta s} + M\frac{di_{\beta r}}{dt},\\
v_x &= (R_s + L_s\frac{d}{dt})i_{xs},\\
v_y &= (R_s + L_s\frac{d}{dt})i_{ys},\\
0 &= (R_r + L_r\frac{d}{dt})i_{\alpha r} + M\frac{di_{\alpha r}}{dt} + \omega_r L_r i_{\beta r} + \omega_r M i_{\beta s},\\
0 &= (R_r + L_r\frac{d}{dt})i_{\beta r} + M\frac{di_{\beta r}}{dt} + \omega_r L_r i_{\alpha r} - \omega_r M i_{\alpha s},\\
T_e &= 3pM(i_{\beta r}i_{\alpha s} - i_{\alpha r}i_{\beta s}),
\end{aligned}
\tag{4}
$$

where $L_s = L_{ls} + M$, $L_r = L_{lr} + M$, $M = 3L_m$, and $\omega_r = p\omega_m$ are p, and ω_m is the pole pairs number and the mechanical speed, respectively. Furthermore, the indices r and s denote rotor and stator values, while subscript l and m denote leakage and magnetizing inductance, respectively.

Due to the effects of the Clarke transformation in the presented topology, the switching states can be classified in five different groups according to the module of the voltage vectors in the primary subspace: large (V_l), medium-large (V_{ml}), medium (V_m), small (V_s), and null (V_0) vectors [34,35]. This classification is represented in Figure 2. An interesting relation can be observed by comparing the modules of the voltage vectors in the α-β and the x-y plane. Particularly, V_l (colored in blue) presents a notable production in the primary subspace, with the smallest production in the secondary plane. This fact makes them especially suitable for use, since a high degree of exploitation of the dc-bus and small copper losses are desirable control traits [4]. For that reason, these switching states are the ones accessible by the control methods studied in this proposal along with V_0 (colored in white).

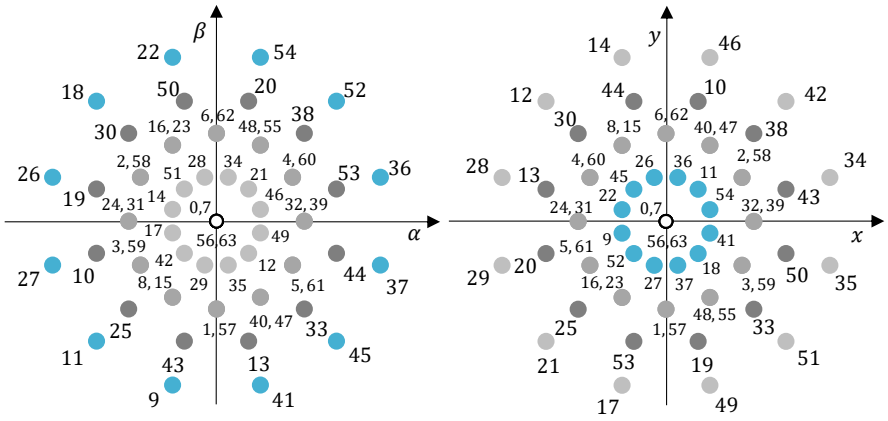


Figure 2. Classification of available control actions in the α-β and x-y planes, with V_l highlighted in blue.

Following with the modification of reference frames, each subspace can be projected again to decouple the flux/torque production through the use of the rotation matrix known as Park transformation (5) once the rotor flux angle (θ) is obtained by means of the measured speed and estimated slip [36]. Through the use of this transformation, flux production is only related to the d-component, while the q-component is linked to torque generation, which eases the implementation of control schemes.

$$
[D] = \begin{bmatrix} cos\theta & sin\theta \\ -sin\theta & cos\theta \end{bmatrix}. \tag{5}
$$

3. FCS-MPC

3.1. FCS-MPC Structure

The FCS-MPC scheme constitutes two control loops, as shown in Figure 3. The external control loop regulates speed through the use of a proportional–integral controller, assessing the present mechanical speed thanks to an encoder and comparing it with its reference counterpart (see the bottom part of Figure 3). On the other hand, the internal control loop is based on the equations that describe the machine model and has the objective of predicting future stator currents in order to regulate them. The expression (6) presents the machine model in space vector variables:

$$\begin{aligned} \frac{d}{dt}\left[X_{\alpha\beta xy}\right] &= [A]\left[X_{\alpha\beta xy}\right] + [B]\left[U_{\alpha\beta xy}\right], \\ \left[U_{\alpha\beta xy}\right] &= \begin{bmatrix} v_{\alpha s} & v_{\beta s} & v_{xs} & v_{ys} & v_{0+} & v_{0-} \end{bmatrix}^T, \\ \left[X_{\alpha\beta xy}\right] &= \begin{bmatrix} i_{\alpha s} & i_{\beta s} & i_{xs} & i_{ys} & \lambda_{\alpha r} & \lambda_{\beta r} \end{bmatrix}^T, \end{aligned} \tag{6}$$

where matrices $[A]$ and $[B]$ depict the dynamic behavior of the six-phase IM [27]. The terms $\lambda_{\alpha r}$ and $\lambda_{\beta r}$ refer to the rotor flux production mapped onto the α-β subspace. The equations in (6) have been discretized through the use of the Euler forward method in order to simplify implementation.

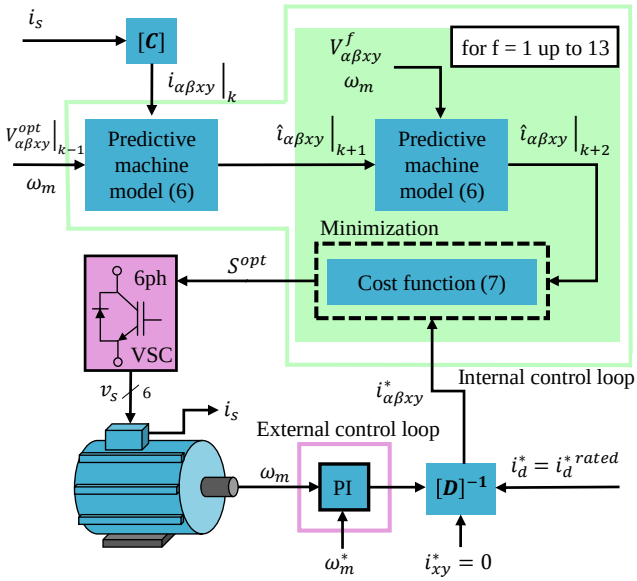


Figure 3. Diagram of a standard FCS-MPC scheme for a six-phase electric drive, with its predictive control loop highlighted in green.

For the purpose of satisfying the real-time requirements that are in place when predicting the stator currents using a digital signal processor, the one-step delay approach is implemented [37]. Therefore, the prediction is performed two steps into the future $(k+2)$, with this being the moment in which the currents produced by the available control actions are compared with their reference counterparts, denoted by the superscript "$*$". The reference value of the quadrature current (i^*_q) is provided by the external control loop, while i^*_d is set to the value that generates rated magnetization. These currents are projected onto the α-β subspace and, along with i^*_x and i^*_y (which are usually set to zero to mitigate copper losses), are included in a cost function. The objective of this function is to select the optimal available control action through the minimization of the total error:

$$J = e^2_{\alpha s} + e^2_{\beta s} + K_{xy}(e^2_{xs} + e^2_{ys}), \tag{7}$$

where

$$\begin{aligned} e_{\alpha s} &= i^*_{\alpha s}|_{k+2} - \hat{\imath}_{\alpha s}|_{k+2}, \\ e_{\beta s} &= i^*_{\beta s}|_{k+2} - \hat{\imath}_{\beta s}|_{k+2}, \\ e_{xs} &= i^*_{xs}|_{k+2} - \hat{\imath}_{xs}|_{k+2}, \\ e_{ys} &= i^*_{ys}|_{k+2} - \hat{\imath}_{ys}|_{k+2}, \end{aligned} \tag{8}$$

with K_{xy} being a weighting factor designed to regulate control goals. Through the comparison between the reference and predicted currents (designated by the circumflex accent on the i, "ˆ"), the cost function estimates the optimal switching state (S_{opt}) for the future instant $k+2$. Figure 3 outlines the algorithm followed by the FCS-MPC. In it, the superscript "f" is used to signal the different iterations performed to minimize the cost function, one per control action available. In the present case, these actions are V_0 and the twelve V_l, for a total of thirteen.

3.2. The Limits of the Standard Cost Function

It must be noted that the expression described in (7) has the objective of minimizing the sum of four different errors, but could allow for an individual increase in some of the components as long as the other errors compensate the value of the sum. In order to better illustrate this fact, experimental tests were performed at a mechanical speed of 800 rpm and a sampling frequency of 20 kHz. Figure 4 displays the squared values of the errors for both the primary subspace (Figure 4a) and the secondary one (Figure 4b and the zoom in Figure 4c), in which the errors are multiplied by the weighting factor (K_{xy}) to more accurately describe the perception of the cost function. The value of K_{xy} has been set heuristically to reduce copper losses without compromising current tracking in the primary subspace. Nevertheless, it can be observed how the algorithm favors control actions that permit a notable increase in either e^2_{xs} or e^2_{ys} during many cycles (see the red stars in Figure 4b). This behavior leads to an excessive and undesirable accumulation of the error in one of the components, a fact that can be better appreciated in Figure 4c, which is a zoom of the section marked in grey in Figure 4b. Here, it is clear how the errors accumulate between sampling periods despite the efforts made by the cost function to keep the sum to a minimum. In other words, the tendency of individual errors to grow is not compensated because the cost function is actually blind to it. As it stands, the algorithm only focuses on the sum of the errors, not on their individual values or how they change through time.

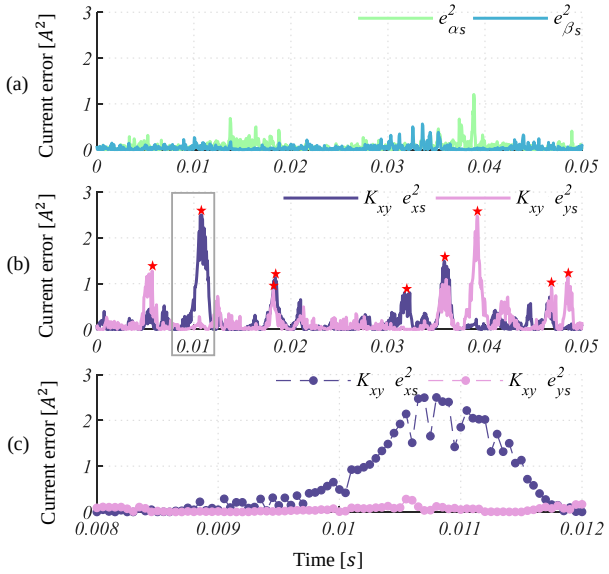


Figure 4. Experimental measurements of errors in a standard FCS-MPC scheme. (**a**) Squared errors in the primary plane, (**b**) squared errors in the secondary plane, and (**c**) zoom of the squared errors in the secondary plane.

4. Compensation of Accumulated Current Errors

4.1. The Proposed Solution: RAE-MPC

Thanks to the error analysis developed in Section 3, a flaw in the FCS-MPC's behavior has been detected. However, one of the interesting capabilities of this type of controller is their inherent flexibility, which has been used in previous works to achieve different control objectives. Some examples are enhancing current tracking [28,38], decreasing the VSC switching frequency [29] or mitigating common-mode voltages [30,39]. It extends to reason that, by modifying (7) in such a manner that the individual accumulative errors of the different components are limited, a significant improvement in terms of reference tracking can be achieved. The enhancement would be especially noticeable in the secondary subspace, where the components becomes more sensitive due to the low impedance of this plane. Therefore, the underlying idea of the proposal is to find a method to diminish the high peak values observed in the preliminary test caused by the accumulation of notable errors during many cycles.

To this end, the present work redefines the common cost function with the addition of a memory stage in order to reduce the accumulated error during the MPC's performance. The inner loop of the proposed control is described in Figure 5. The memory stage consists of a "first in first out" (FIFO) queue, which stores the difference between reference currents and the ones predicted by the algorithm for $k+2$ during the last two cycles. These values are later added up to provide a measurement of the tendency of each component in the past, following this expression:

$$\begin{aligned} e_{\alpha s}^{ms} &= e_{\alpha s}^{'} + e_{\alpha s}^{''} \\ e_{\beta s}^{ms} &= e_{\beta s}^{'} + e_{\beta s}^{''} \\ e_{xs}^{ms} &= e_{xs}^{'} + e_{xs}^{''} \\ e_{ys}^{ms} &= e_{ys}^{'} + e_{ys}^{''} \end{aligned} \tag{9}$$

where the superscripts "$'$" and "$''$" refer to the current errors produced by the optimal control actions estimated in the last cycle and two cycles ago, respectively. During the control action selection, these past errors are added to the ones produced by the vector being evaluated (designated with the superscript "f"):

$$\begin{aligned} e_{\alpha s}^{acc} &= e_{\alpha s}^{f} + e_{\alpha s}^{ms}, \\ e_{\beta s}^{acc} &= e_{\beta s}^{f} + e_{\beta s}^{ms}, \\ e_{xs}^{acc} &= e_{xs}^{f} + e_{xs}^{ms}, \\ e_{ys}^{acc} &= e_{ys}^{f} + e_{ys}^{ms}. \end{aligned} \tag{10}$$

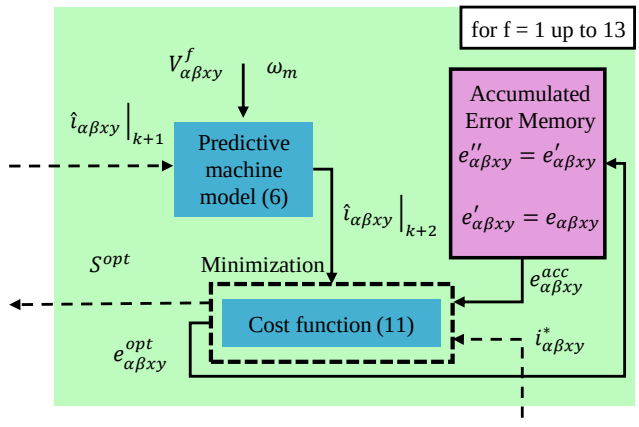


Figure 5. Control loop of the proposed RAE-MPC scheme.

The accumulated errors are finally included in the designed cost function and regulated through the use of a weighting factor (K_{acc}) as follows:

$$J = e_{\alpha s}^2 + e_{\beta s}^2 + K_{xy}(e_{xs}^2 + e_{ys}^2) + K_{acc}\, e_{\alpha\beta xy}^{acc2}, \tag{11}$$

where

$$e_{\alpha\beta xy}^{acc2} = (e_{\alpha s}^{acc})^2 + (e_{\beta s}^{acc})^2 + (e_{xs}^{acc})^2 + (e_{ys}^{acc})^2. \tag{12}$$

With the objective of more clearly depicting the control action selection algorithm, Figure 6 is presented.

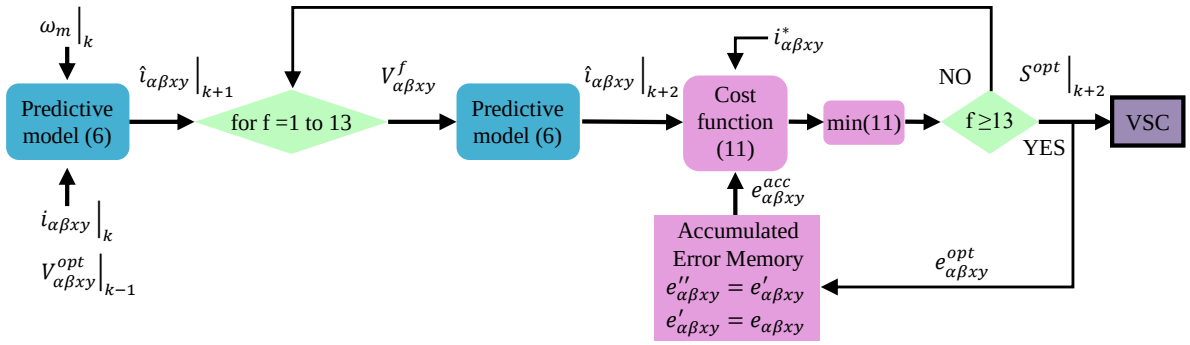


Figure 6. RAE-MPC switching state selection process.

4.2. RAE-MPC Conceptual Behavior

Furthermore, a qualitative example of the internal workings of the algorithm is displayed in Figure 7. The left graph presents the evolution of the errors for a scheme governed by the cost function of a standard FCS-MPC, as depicted in (7). It can be observed how the error in the x component grows notably over time in a similar fashion to Figure 4. In the present cycle, this fact is explained by the selection of V_1 as the optimal control action. Even though its error in x is high, the error in the other components would be low enough to minimize J. In contrast, the right graph shows the effect that a simplification of the proposed control method would have in the studied component. More concretely, it has been considered that the cost function only takes into account the accumulated current error for the sake of clarity. As it can be observed, the recorded errors in x for two (e''_{xs}) and one (e'_{xs}) cycles ago are 1 A and 3 A, respectively. Therefore, the accumulated error in the memory stage (e_{xs}^{ms}) is their sum, 4 A. According to (10), the optimal switching state in terms of the x component would be the one that obtains the error closest to $-e_{xs}^{ms}$, depicted as a white dot in the graph. This variation is responsible for the change in chosen control action, which is now V_3 instead of V_1. As a consequence, the accumulation of the error in the x component is avoided.

It is worth noting that the selection performed by the proposed method is more complex than the one depicted in Figure 7, since the optimization of the accumulated errors is carried out in the four currents. Furthermore, the cost function is actually the sum of the two shown in the example, as described in (11). For that reason, a compromise between obtaining a small sum of errors and minimizing accumulated individual errors is expected.

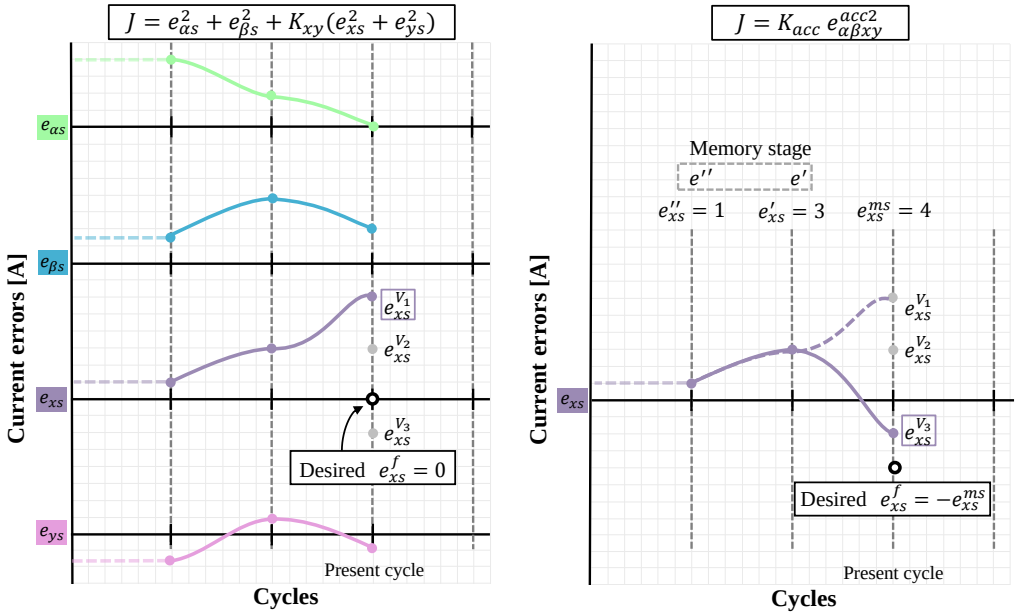


Figure 7. Example of the effects of the RAE-MPC in the desired current errors.

5. Experimental Results

5.1. Experimental Rig

The test bench employed to obtain the experimental results of the proposed RAE-MPC is presented in Figure 8. The electric drive is formed by a six-phase IM connected to dual two-level three-phase VSCs (Semikron SKS22F), fed by a single dc-link. Regarding the control system, it is based on a digital signal processor from Texas Instrument (TMS320F28335), programmed using a JTAG and the software Code Composer Studio v5.3.0. The sensor setup comprises four hall effect probes (LEM LAH 25NP) and an encoder (GHN510296R) in order to measure stator currents and mechanical speed, respectively. To provide a load torque to the six-phase IM, its shaft is coupled to a dc-machine working as a generator. The armature of the dc-machine is connected to a variable passive load with the objective of dissipating power, making the load speed-dependent. Table 1 presents a summary of the test rig parameters, which have been obtained using ac time domain and standstill with inverter supply tests [40,41].

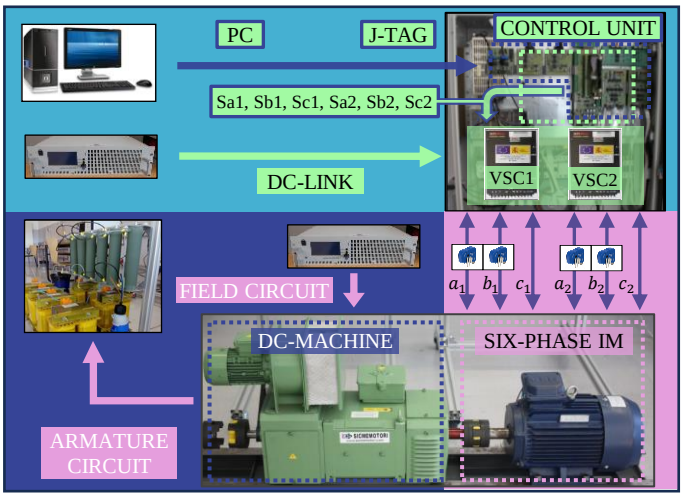


Figure 8. Diagram of the experimental test bench used to assess the control performance.

Table 1. Six-phase IM drive parameters.

Parameter		Value
V_{dc} (V)	dc-link voltage	300
T_{rated} (Nm)	Rated torque	8
R_s (Ω)	Stator resistance	4.20
R_r (Ω)	Rotor resistance	3
L_m (mH)	Mutual inductance	370
L_{ls} (mH)	Stator leakage inductance	4.5
L_{lr} (mH)	Rotor leakage inductance	55.12

5.2. Experimental Tests

The present section details the experimental tests carried out to demonstrate the suitable performance of the RAE-MPC when compared to an MPC based on the use of V_l vectors as active control actions. The improvements are presented in two manners. On the one hand, diverse quality indices are employed to compare both control solutions, such as the total harmonic distortion (THD) of phase currents, peak-to-peak currents in the secondary subspace (I_{xy}^{p2p}), the maximum squared error of the currents in the secondary subspace multiplied by its weighting factor (e_{xy}^{2max}), and the obtained switching frequency (f_{sw}). These indices have been calculated for different operating points and sampling frequencies (f_s) in an effort to demonstrate the flexibility of the proposed method. On the other hand, the tracking of the different control variables are depicted. Its objective is to present visual proof of the enhanced performance provided by the RAE-MPC. Furthermore, since the proposed method requires the tuning of a new weighting factor, a study on the complexity of this adjustment has been performed.

With the intention of obtaining the quality indices used to compare the MPC and the proposed RAE-MPC, tests have been performed at two different mechanical speeds (500 and 800 rpm) and two sampling frequencies (10 kHz in Table 2 and 20 kHz in Table 3). The improvements achieved by the presented method can be observed from various perspectives. First of all, RAE-MPC displays significantly lower values of THD in all speeds and values of f_s. In the case of $f_s = 10$ kHz, current THD diminishes from 37.67% to 26.63% for a relative improvement of -29.31% at 500 rpm, whereas at higher speeds (800 rpm) THD drops from 30.62% to 22.64%, a relative reduction of 26.06%. This enhancement in performance is also present at $f_s = 20$ kHz, where the relative reduction in harmonic content is 26.20% at 500 rpm and a remarkable 35.69% at 800 rpm.

Table 2. Quality indices in a range for $f_s = 10$ kHz.

ω (rpm)	Method	THD (%)	I_{xy}^{p2p} (A)	e_{xy}^{2max} (A^2)	f_{sw} (kHz)
500	MPC	37.67	4.34	4.36	2.79
500	RAE	26.63	3.29	0.57	2.94
800	MPC	30.62	4.62	6.60	2.34
800	RAE	22.64	3.40	0.58	2.29

Table 3. Quality indices in a range for $f_s = 20$ kHz.

ω (rpm)	Method	THD (%)	I_{xy}^{p2p} (A)	e_{xy}^{2max} (A^2)	f_{sw} (kHz)
500	MPC	26.76	3.39	2.09	5.65
500	RAE	19.75	2.24	0.27	5.94
800	MPC	21.66	3.49	4.98	4.43
800	RAE	15.11	2.42	0.27	4.38

The improvement in the current harmonic content can be explained by the different performance of the MPC and RAE-MPC in controlling the secondary subspace. By observ-

ing I_{xy}^{p2p} values, it is clear that the proposed method is successful at reducing peak currents when $f_s = 10$ kHz (going from 4.34 A to 3.29 A at 500 rpm and from 4.62 A to 3.40 A at 800 rpm) and also $f_s = 20$ kHz (going from 3.39 A to 2.24 A at 500 rpm and from 3.49 A to 2.42 A at 800 rpm). In all cases, a reduction of more than 24% is achieved, thus leading to lower copper losses.

At a lower sampling frequency, RAE-MPC reduces by 7.65 times the value of the maximum squared current error measured at 500 rpm and by 11.38 times at 800 rpm. In the case of $f_s = 20$ kHz, this quality index is 7.74 times smaller at 500 rpm and 18.44 at 800 rpm. It must be noted that the achieved reduction in currents in the secondary plane does not come from increasing the number of switching states applied per control period, but from the correct minimization of the accumulative error. The tests performed at a sampling frequency of 20 kHz are illustrated in Figure 9 (500 rpm) and Figure 10 (800 rpm).

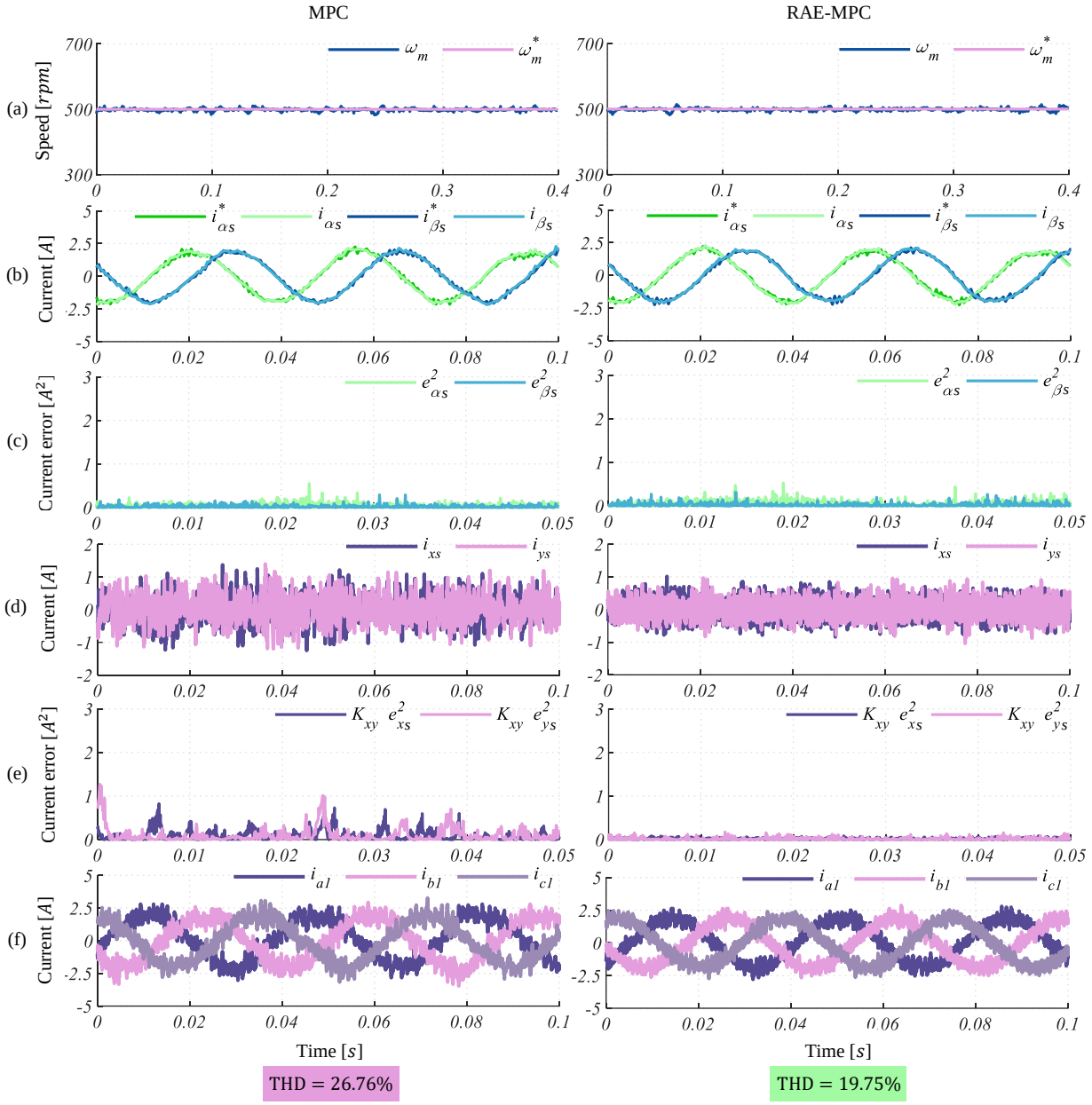


Figure 9. Speed (**a**), α-β currents (**b**), α-β squared errors (**c**), x-y currents (**d**), x-y squared errors multiplied by their weighting factor (**e**), and phase currents (**f**) when $f_s = 20$ kHz and $\omega = 500$ rpm.

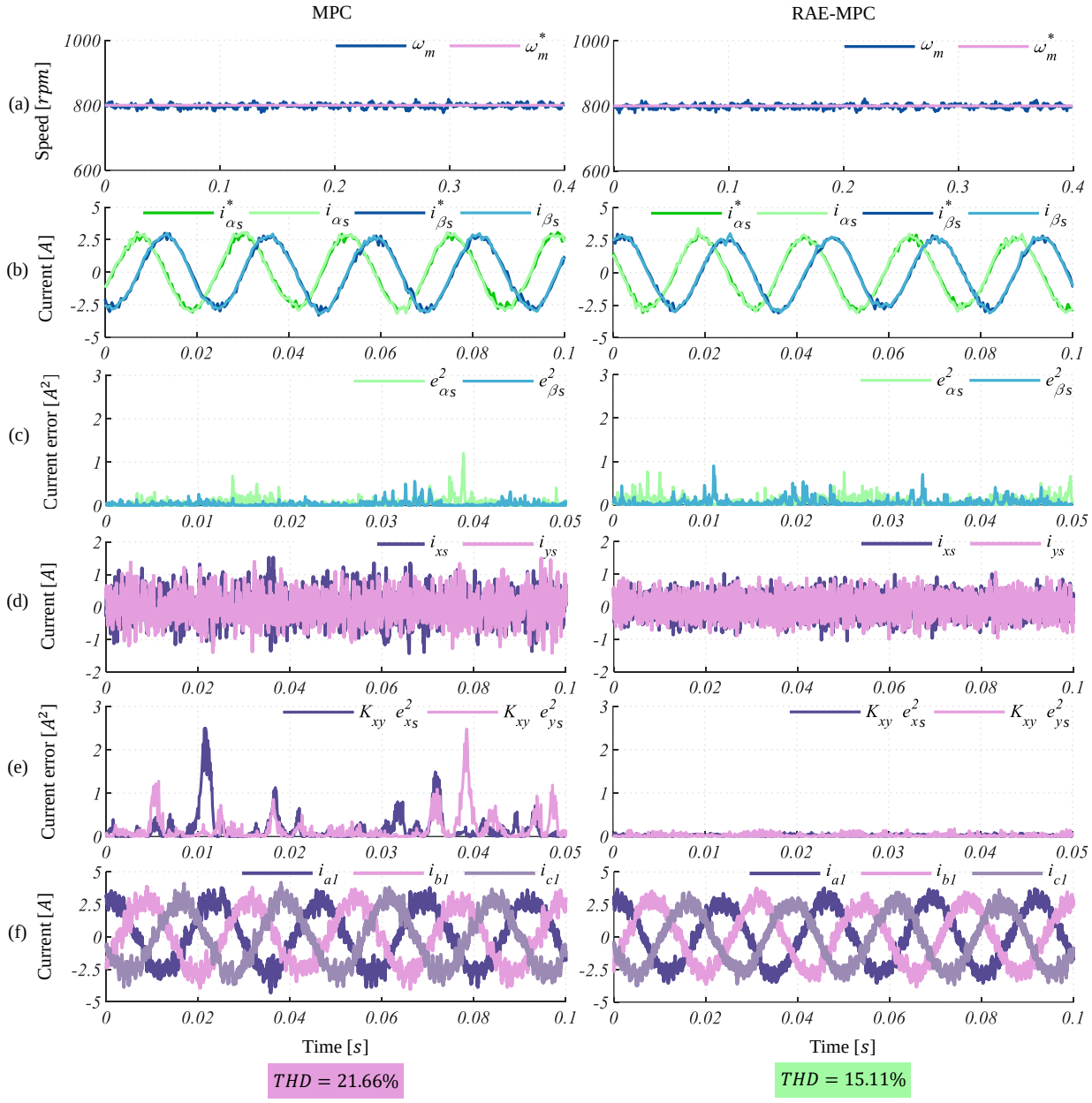


Figure 10. Speed (**a**), α-β currents (**b**), α-β squared errors (**c**), x-y currents (**d**), x-y squared errors multiplied by their weighting factor (**e**), and phase currents (**f**) when $f_s = 20$ kHz and $\omega = 800$ rpm.

In both cases, it can be appreciated how the reference values of speed (Figures 9a and 10a) and currents in the primary subspace (Figures 9b and 10b) are correctly followed by the two compared methods. As a consequence of the adequate tracking in the primary plane, its squared error (Figures 9c and 10c) is small in all the studied cases. However, different behavior is observed when studying the currents in the secondary plane (Figures 9d and 10d) and its squared error (Figures 9e and 10e). The accumulated error through time, manifesting in notable peaks present during the whole test at both speeds, is clearly compensated when using RAE-MPC. Furthermore, the graphs in both Figures 9e and 10e complement the information given by the quality index e_{xy}^{2max}. It is noticeable how considering the accumulated error in the cost function not only reduces the peak value registered of these errors, but it also diminishes the errors during the whole test, which translates into less distorted phase currents (Figures 9f and 10f). Once again, it should be noted that this improvement is achieved without compromising the tracking of primary currents, which

is an attainment that cannot be accomplished by increasing the value of K_{xy} in standard FCS-MPC.

Since the primary objective of including the accumulated error in the cost function is to enhance current quality, the study of current THD has been extended in Figure 11. The values of this quality index are presented for both MPC and RAE-MPC at three different speeds and control frequencies, with the proposed method displaying lower current distortion in all the tested conditions.

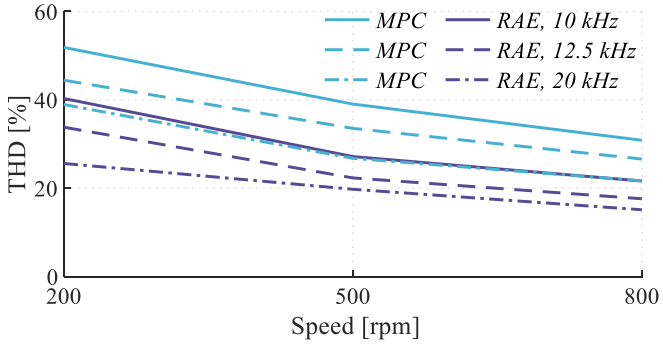


Figure 11. Current THD values obtained by standard MPC and RAE-MPC across different control frequencies (10, 12.5, and 20 kHz) and speeds (200, 500, and 800 rpm).

A possible disadvantage to the proposed method is the increase in computational effort. The time that the microcontroller requires to perform all the operations that form the regulation scheme set a hard limit to the achievable control frequency. However, it should be remarked that RAE-MPC only requires the inclusion of low-cost mathematical operations. By experimentally measuring the benchmark FCS-MPC approach time in the test rig, the algorithm requires 28 µs, while the proposed RAE-MPC needs 32 µs. This increase, although measurable, can be considered acceptable when compared to the benefits that the proposed scheme provides.

In summary, the performance shown by RAE-MPC at various sampling frequencies and points of operation demonstrates the value of compensating the accumulated current errors. While traditional FCS-MPC targets only the sum of all errors, the proposed method achieves significantly lower harmonic distortion and copper losses by including in the cost function a term that reflects the past evolution of the individual components. As a consequence, the algorithm favors the usage of control actions that compensate the tendencies of growth in each component, especially in the secondary plane due to its high sensitivity. Furthermore, the benefits of this method come without compromising dc-link usage, current tracking in the primary plane or an increase in switching frequency and subsequent switching losses.

5.3. Weighting Factor Influence

Traditional FCS-MPC in multi-phase machines requires the appropriate tuning of one weighting factor for every secondary subspace. In the cost function presented in (7), the value of K_{xy} must be adjusted to accommodate two control goals: tracking the reference values of α-β currents and lowering the production of x-y currents. On the other hand, the implementation of RAE-MPC requires the adjustment of an additional parameter, K_{acc}. As the weighting factors of the cost function tend to be adjusted heuristically, the proposed method adds a new degree of complexity. In principle, RAE-MPC presents the disadvantage of requiring more tuning tests in order to achieve the optimal performance. To approximate the importance of this disadvantage, multiple tests have been performed, maintaining the operating point ($f_s = 20$ kHz, $\omega = 800$ rpm) but modifying the value of K_{xy} and K_{acc} in (11). Both parameters have been adjusted individually, meaning that the results for the study of K_{xy} are obtained with $K_{acc} = 0$, and vice versa.

With the objective of displaying the effects of these weighting factors on harmonic injection and current reference tracking in the primary subspace, Figure 12 is presented. The left graph of Figure 12 shows the evolution of THD, which is related to current production in the secondary subspaces. As it can be seen, both factors are inversely proportional to this quality index. While a value of 0.05 in K_{xy} produces a THD of 24.53 %, increasing it up to 2 reduces it to 16.54 %. Similarly, these values applied to K_{acc} obtain 17.11 % and 12.69 %, respectively. However, low harmonic injection is not desirable if it comes at the cost of a poor tracking of the references. In order to monitor this tracking, the Root Mean Squared Error between the reference and the measured currents in the primary subspace ($RMSE_{\alpha\beta}$) has been plotted on the right graph of Figure 12. Here, the opposite tendency is observed: increasing the priority of secondary control goals worsens the quality index. However, the two studied factors increase the error at notably different rates. Both start with an $RMSE_{\alpha\beta}$ of approximately 0.21 A when each weighting factor has a value of 0.05, but once K_{xy} is increased up to 2, $RMSE_{\alpha\beta}$ reaches 0.52 A. On the other hand, raising K_{acc} only increases $RMSE_{\alpha\beta}$ up to 0.27 A.

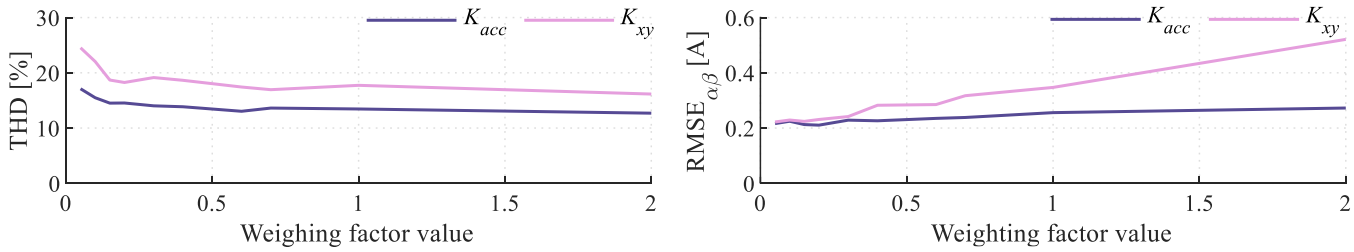


Figure 12. Impact of the value of the weighting factors on THD value (**left**) and $RMSE_{\alpha\beta}$ (**right**).

Two conclusions can be derived from this analysis. Firstly, K_{acc} is more impactful than K_{xy} in the pursuit of low harmonic injection. Secondly, K_{acc} is more stable than K_{xy} and, thus, easier to tune. Notably, an increment of 40 times the original value of the weighting factor introduced by RAE-MPC only amounts to an increase 0.06 A in tracking error, while K_{xy} produces 0.31 A. In summary, although RAE-MPC requires the tuning of one more weighting factor than FCS-MPC, adjusting its value is more straightforward than tuning the standard K_{xy}. This is due to the wide range of values of K_{acc} that provide similar performance quality.

6. Conclusions

The FCS-MPC is considered as a viable alternative to conventional lineal controllers by the research community. The usage of a cost function permits selecting the optimal control action in each sampling period according to the predefined control goals. A common trend in this regard is the use of a cost function focused on the minimization of the total current error. However, this approach entails that the individual error of one of the available components can reach undesired values, disturbing the current quality. Fortunately, the inclusion of a term based on the accumulated error of each component can provide a notable improvement from the perspective of current quality without increasing the number of switching states applied during the control period. For instance, in a high speed scenario, the proposed RAE-MPC achieves a relative reduction in THD of around 35% when a 20 kHz sampling frequency is implemented. Future works could explore the effects of the proposed method on machines with different parameters and higher number of phases, offering the chance of studying the sensitivity of the new secondary subspaces to compensate for the accumulated error. Furthermore, the implementation on systems that allow for higher switching and control frequencies may present an interesting paradigm shift in the behavior of secondary currents and how to reduce them.

Author Contributions: Conceptualization, J.C.-R., I.G.-P. and M.J.D.; methodology, J.C.-R. and I.G.-P.; software, J.C.-R., I.G.-P. and Á.G.-P.; validation, J.C.-R., I.G.-P. and M.J.D.; formal analysis, J.C.-R. and I.G.-P.; investigation, J.J.A., Á.G.-P. and J.C.-R.; resources, I.G.-P. and J.J.A.; data curation, J.C.-R., I.G.-P., Á.G.-P., M.J.D. and J.C.-R.; writing—original draft preparation, J.C.-R. and I.G.-P.; writing—review and editing, Á.G.-P. and J.J.A.; visualization, J.J.A., Á.G.-P. and J.C.-R.; supervision, J.C.-R., I.G.-P. and M.J.D.; project administration, I.G.-P. and M.J.D.; funding acquisition, I.G.-P. and M.J.D. All authors have read and agreed to the published version of the manuscript.

Funding: This research was funded in part by the Spanish Government under the *Plan Estatal* with the reference PID2021-127131OB-I00, in part by *Proyectos Estratégicos Orientados a la Transición Ecológica y a la Transición Digital* under the reference TED2021-129558B-C21 and in part by the *Junta de Andalucía* under the reference UMA20-FEDERJA-039.

Institutional Review Board Statement: Not applicable.

Informed Consent Statement: Not applicable.

Data Availability Statement: Data is contained within the article.

Conflicts of Interest: The authors declare no conflicts of interest.

Abbreviations

The following abbreviations are used in this manuscript:

FCS-MPC	Finite Control Set Model Predictive Control.
RAE-MPC	Reduced-Accumulated Error Model Predictive Control.
VSC	Voltage Source Converter.
IM	Induction Machine.
VSD	Vector Space Decomposition.
FIFO	First In First Out.
THD	Total Harmonic Distortion.
RMSE	Root Mean Squared Error.

References

1. Levi, E.; Bojoi, R.; Profumo, F.; Toliyat, H.; Williamson, S. Multiphase induction motor drives—A technology status review. *Electr. Power Appl. IET* **2007**, *1*, 489–516. [CrossRef]
2. Levi, E. Multiphase Electric Machines for Variable-Speed Applications. *IEEE Trans. Ind. Electron.* **2008**, *55*, 1893–1909. [CrossRef]
3. Salem, A.; Narimani, M. A Review on Multiphase Drives for Automotive Traction Applications. *IEEE Trans. Transp. Electrif.* **2019**, *5*, 1329–1348. [CrossRef]
4. Duran, M.J.; Gonzalez-Prieto, I.; Gonzalez-Prieto, A.; Aciego, J.J. The Evolution of Model Predictive Control in Multiphase Electric Drives: A Growing Field of Research. *IEEE Ind. Electron. Mag.* **2022**, *16*, 29–39. [CrossRef]
5. Levi, E. Advances in Converter Control and Innovative Exploitation of Additional Degrees of Freedom for Multiphase Machines. *IEEE Trans. Ind. Electron.* **2016**, *63*, 433–448. [CrossRef]
6. Frikha, M.A.; Croonen, J.; Deepak, K.; Benômar, Y.; El Baghdadi, M.; Hegazy, O. Multiphase Motors and Drive Systems for Electric Vehicle Powertrains: State of the Art Analysis and Future Trends. *Energies* **2023**, *16*, 768. [CrossRef]
7. Abdel-Moneim, M.G.; Abdel-Azim, W.E.; Abdel-Khalik, A.S.; Hamed, M.S.; Ahmed, S. Model Predictive Current Control of Nine-Switch Inverter-Fed Six-Phase Induction Motor Drives Under Healthy and Fault Scenarios. *IEEE Trans. on Trans. Electrif.* **2024**. [CrossRef]
8. Su, J.; Gao, R.; Husain, I. Model Predictive Control Based Field-Weakening Strategy for Traction EV Used Induction Motor. *IEEE Trans. Ind. Appl.* **2018**, *54*, 2295–2305. [CrossRef]
9. BMW iX M60. Available online: https://www.bmw.co.uk/en/all-models/m-models/bmw-ix-m60/2021/bmw-ix-m60-highlights.html (accessed on 11 December 2024).
10. Mercedes AMG EQS 53. Available online: https://www.mercedes-amg.com/en/world-of-amg/news/press-information/mercedes-amg-eqs-53.html (accessed on 11 December 2024).
11. Audi QE-Tron. Available online: https://www.audi-mediacenter.com/en/audi-at-the-dakar-rally-2023-15116/technical-data-audi-rs-q-e-tron-dakar-2023-15119 (accessed on 11 December 2024).
12. Furmanik, M.; Gorel, L.; Konvičný, D.; Rafajdus, P. Comparative Study and Overview of Field-Oriented Control Techniques for Six-Phase PMSMs. *Appl. Sci.* **2021**, *11*, 7841. [CrossRef]
13. Iffouzar, K.; Amrouche, B.; Otmane Cherif, T.; Benkhoris, M.F.; Aouzellag, D.; Ghedamsi, K. Improved direct field oriented control of multiphase induction motor used in hybrid electric vehicle application. *Int. J. Hydrogen Energy* **2017**, *42*, 19296–19308. [CrossRef]

14. Bojoi, R.; Farina, F.; Griva, G.; Profumo, F.; Tenconi, A. Direct torque control for dual three-phase induction motor drives. *IEEE Trans. Ind. Appl.* **2005**, *41*, 1627–1636. [CrossRef]
15. Bermudez, M.; Barrero, F.; Martin, C.; Perales, M. Performance Analysis of Direct Torque Controllers in Five-Phase Electrical Drives. *Appl. Sci.* **2021**, *11*, 11964. [CrossRef]
16. Mamdouh, M.; Abido, M.A. Simple Predictive Current Control of Asymmetrical Six-Phase Induction Motor with Improved Performance. *IEEE Trans. Ind. Electron.* **2023**, *70*, 7580–7590. [CrossRef]
17. Rodriguez, J.; Garcia, C.; Mora, A.; Davari, S.A.; Rodas, J.; Valencia, D.F.; Elmorshedy, M.; Wang, F.; Zuo, K.; Tarisciotti, L.; et al. Latest Advances of Model Predictive Control in Electrical Drives—Part II: Applications and Benchmarking with Classical Control Methods. *IEEE Trans. Power Electron.* **2022**, *37*, 5047–5061. [CrossRef]
18. Kodumur Meesala Ravi Eswar, K.V.P.K.; Kumar, T.V. Enhanced Predictive Torque Control with Auto-Tuning Feature for Induction Motor Drive. *Electr. Power Compon. Syst.* **2018**, *46*, 825–836. [CrossRef]
19. Yu, B.; Song, W.; Yang, K.; Guo, Y.; Saeed, M.S.R. A Computationally Efficient Finite Control Set Model Predictive Control for Multiphase PMSM Drives. *IEEE Trans. Ind. Electron.* **2022**, *69*, 12066–12076. [CrossRef]
20. Gonçalves, P.F.C.; Cruz, S.M.A.; Mendes, A.M.S. Multistage Predictive Current Control Based on Virtual Vectors for the Reduction of Current Harmonics in Six-Phase PMSMs. *IEEE Trans. Energy Convers.* **2021**, *36*, 1368–1377. [CrossRef]
21. Luo, Y.; Liu, C. Multi-Vector-Based Model Predictive Torque Control for a Six-Phase PMSM Motor with Fixed Switching Frequency. *IEEE Trans. Energy Convers.* **2019**, *34*, 1369–1379. [CrossRef]
22. Zhao, W.; Wang, H.; Tao, T.; Xu, D. Model Predictive Torque Control of Five-Phase PMSM by Using Double Virtual Voltage Vectors Based on Geometric Principle. *IEEE Trans. Transp. Electrif.* **2021**, *7*, 2635–2644. [CrossRef]
23. Xue, C.; Song, W.; Feng, X. Finite control-set model predictive current control of five-phase permanent-magnet synchronous machine based on virtual voltage vectors. *IET Electr. Power Appl.* **2017**, *11*, 836–846. [CrossRef]
24. Sun, J.; Yang, Y.; Chen, R.; Zhang, X.; Lim, C.S.; Rodriguez, J. An Efficient Multi-Vector-Based Model Predictive Current Control for PMSM Drive. *CPSS Trans. Power Electron. Appl.* **2024**, *9*, 79–89. [CrossRef]
25. Parvathy, M.L.; Kumar, T.V. A Multivector-Based Model Predictive Current Control of PMSM Drive with Enhanced Torque and Flux Response. *IEEE J. Emerg. Sel. Top. Power Electron.* **2022**, *10*, 7527–7538. [CrossRef]
26. da Paz, G.F.; Melo, V.F.M.B.; de Freitas, I.S.; de Sousa, R.P.R.; Salvadori, F. Virtual Vector Direct Torque Control for a Nine-Phase Induction Machine Drive System with Eight Active Voltage Vectors Emulating Virtual Voltage Vectors. *IEEE Trans. Power Electron.* **2024**, *39*, 9457–9469. [CrossRef]
27. Aciego, J.J.; Gonzalez-Prieto, I.; Duran, M.J.; Gonzalez-Prieto, A.; Carrillo-Rios, J. Guiding the Selection of Multi-Vector Model Predictive Control Techniques for Multiphase Drives. *Machines* **2024**, *12*, 115. [CrossRef]
28. Arahal, M.R.; Martín, C.; Kowal, A.; Castilla, M.; Barrero, F. Cost function optimization for predictive control of a five-phase IM drive. *Optim. Control Appl. Methods* **2020**, *41*, 84–93. [CrossRef]
29. Ayala, M.; Doval-Gandoy, J.; Rodas, J.; Gonzalez, O.; Gregor, R. Current control designed with model based predictive control for six-phase motor drives. *ISA Trans.* **2020**, *98*, 496–504. [CrossRef]
30. Duran, M.J.; Riveros, J.A.; Barrero, F.; Guzman, H.; Prieto, J. Reduction of Common-Mode Voltage in Five-Phase Induction Motor Drives Using Predictive Control Techniques. *IEEE Trans. Ind. Appl.* **2012**, *48*, 2059–2067. [CrossRef]
31. Slunjski, M.; Dordevic, O.; Jones, M.; Levi, E. Symmetrical/Asymmetrical Winding Reconfiguration in Multiphase Machines. *IEEE Access* **2020**, *8*, 12835–12844. [CrossRef]
32. Che, H.S.; Hew, W.P. Dual three-phase operation of single neutral symmetrical six-phase machine for improved performance. In Proceedings of the IECON 2015—41st Annual Conference of the IEEE Industrial Electronics Society, Yokohama, Japan, 9–12 November 2015; pp. 001176–001181.
33. Zhao, Y.; Lipo, T. Space vector PWM control of dual three phase induction machine using vector space decomposition. In Proceedings of the 1994 IEEE Industry Applications Society Annual Meeting, Denver, CO, USA, 2–5 October 1994; Volume 1, pp. 742–749.
34. Serra, J.; Jlassi, I.; Cardoso, A.J.M. A Computationally Efficient Model Predictive Control of Six-Phase Induction Machines Based on Deadbeat Control. *Machines* **2021**, *9*, 306. [CrossRef]
35. Luo, Y.; Niu, S. Predictive Current Control for Six-Phase PMSM Motor with Multi-Step Synthesis Based Virtual Vectors. *IEEE Trans. Energy Convers.* **2023**, *38*, 134–146. [CrossRef]
36. Gonzalez-Prieto, I.; Duran, M.J.; Barrero, F.; Bermudez, M.; Guzman, H. Impact of Postfault Flux Adaptation on Six-Phase Induction Motor Drives with Parallel Converters. *IEEE Trans. Power Electron.* **2017**, *32*, 515–528. [CrossRef]
37. Karamanakos, P.; Liegmann, E.; Geyer, T.; Kennel, R. Model Predictive Control of Power Electronic Systems: Methods, Results, and Challenges. *IEEE Open J. Ind. Appl.* **2020**, *1*, 95–114. [CrossRef]
38. Abbaszadeh, A.; Khaburi, D.A.; Mahmoudi, H.; Rodríguez, J. Simplified model predictive control with variable weighting factor for current ripple reduction. *IET Power Electron.* **2017**, *10*, 1165–1174. [CrossRef]
39. Li, J.; Song, W.; Yue, H.; Sun, N.; Ma, C.; Feng, R. An Improved MPC with Reduced CMV and Current Distortion for PMSM Drives Under Variable DC-Bus Voltage Condition in Electric Vehicles. *IEEE Trans. Power Electron.* **2023**, *38*, 5167–5177. [CrossRef]

40. Yepes, A.G.; Riveros, J.A.; Doval-Gandoy, J.; Barrero, F.; Lopez, O.; Bogado, B.; Jones, M.; Levi, E. Parameter Identification of Multiphase Induction Machines with Distributed Windings—Part 1: Sinusoidal Excitation Methods. *IEEE Trans. Energy Convers.* **2012**, *27*, 1056–1066. [CrossRef]
41. Riveros, J.A.; Yepes, A.G.; Barrero, F.; Doval-Gandoy, J.; Bogado, B.; Lopez, O.; Jones, M.; Levi, E. Parameter Identification of Multiphase Induction Machines with Distributed Windings—Part 2: Time-Domain Techniques. *IEEE Trans. Energy Convers.* **2012**, *27*, 1067–1077. [CrossRef]

Disclaimer/Publisher's Note: The statements, opinions and data contained in all publications are solely those of the individual author(s) and contributor(s) and not of MDPI and/or the editor(s). MDPI and/or the editor(s) disclaim responsibility for any injury to people or property resulting from any ideas, methods, instructions or products referred to in the content.